


S. SCHILT   
J.-P. BESSON  
L. THÉVENAZ

# Near-infrared laser photoacoustic detection of methane: the impact of molecular relaxation

Ecole Polytechnique Fédérale de Lausanne (EPFL), Nanophotonics and Metrology Laboratory,  
1015 Lausanne, Switzerland

Received: 18 April 2005 / Revised version: 13 October 2005  
© Springer-Verlag 2005

**ABSTRACT** A photoacoustic sensor has been developed for trace-gas monitoring using a near-infrared semiconductor laser emitting in the  $2\nu_3$  band of methane at  $1.65\ \mu\text{m}$ . The apparatus was designed for on-line process control in the manufacturing of the novel low-water-peak fibres developed for optical telecommunications. The importance of collisional relaxation processes in the generation of the photoacoustic signal is reported in the particular case of  $\text{CH}_4$  detection in dry  $\text{O}_2$  and  $\text{O}_2\text{-N}_2$  mixtures. The negative influence of these effects results in a strongly reduced and phase-shifted photoacoustic signal, induced by a fast resonant coupling between the vibrational states of methane and oxygen, associated with the slow relaxation of the excited oxygen molecules. An unusual parabolic response of the sensor with respect to the methane concentration has been observed and is discussed. Finally, the beneficial effect of several species, including water vapour and helium, acting as a catalyst to hasten the relaxation of the  $\text{CH}_4\text{-O}_2$  system, is demonstrated.

**PACS** 42.62.Fi; 33.20.Ea; 34.50.Ez

## 1 Introduction

Infrared photoacoustic spectroscopy (PAS) is widely recognized for its high performances in trace-gas monitoring and is one of the most sensitive techniques to measure low gas concentrations at atmospheric pressure [1]. The high sensitivity of PAS mainly results from its zero-background nature, which means that no signal is produced in the absence of an absorbing species. Furthermore, one of the most outstanding features of this technique is its achromaticity: the response of a photoacoustic (PA) sensor, represented by the cell constant (i.e. the PA signal normalized by the laser power and absorption coefficient), is usually independent of the laser excitation wavelength (however, a few exceptions may occur in some particular situations, as will be discussed later). It means that the same PA detector can be used with any type of laser and at any wavelength, from ultraviolet to mid infrared (MIR), with identical performances in terms of cell constant (provided that a suitable window material is used in the PA cell). This is definitively not the case for other high

sensitivity laser spectroscopy techniques, such as wavelength- or frequency-modulation spectroscopy (WMS/FMS), cavity ring-down spectroscopy (CRDS) or intracavity laser absorption spectroscopy (ICLAS), which all make use of optical detection that has poorer performances in the MIR region. Indeed, not only is the sensitivity of MIR photodiodes strongly reduced in comparison to near-infrared (NIR) ones, but also MIR detectors require low-temperature operation and are much more expensive than NIR detectors.

For several years, there has been much interest in the use of NIR semiconductor lasers in PAS, such as distributed-feedback (DFB) lasers mass produced for the optical telecommunications market, whereas, primarily, it has been predominantly implemented using MIR gas lasers ( $\text{CO}$  or  $\text{CO}_2$  lasers). Extreme detection limits, usually in the part-per-billion (ppb) range, have been achieved with gas lasers [2–4], thanks to their high optical power (a few watts) and their emission in the spectral range of strong fundamental rovibrational transitions of many species. Compared to the discrete line-by-line tunability of gas lasers, which requires an accidental coincidence between an absorption feature of the species under investigation and an emission line of the laser, DFB lasers have the advantage of continuous tunability over several nanometres, enabling a precise adjustment of the laser wavelength to the centre of an absorption line. They also offer a suitable line width for high-resolution spectroscopic techniques and their excellent characteristics in terms of output power, single-mode performance, tunability and modulation capabilities (both in intensity and wavelength), combined with their small size, low power consumption and no cooling requirement, make them ideal candidates for the development of reliable miniature PA sensors.

Despite the achromatic property of PAS, the simple substitution of the excitation laser in a PA sensor by another designed to detect a different species is not always that evident. Whereas this change is generally easily realized, as already demonstrated in some publications, for example by replacing a laser diode emitting at  $1362\ \text{nm}$  in a water vapour measuring setup by another one emitting at  $1531\ \text{nm}$  in order to measure ammonia [5], such a simple change can sometimes result in a dramatic loss in sensitivity or in other unusual behaviours. Such undesirable effects may result from an intrinsic characteristic of PAS, i.e. it is an indirect technique. Indeed, the laser optical energy absorbed by the molecules

✉ Fax: +41-21-693-26-14, E-mail: [stephane.schilt@epfl.ch](mailto:stephane.schilt@epfl.ch)

is not directly measured, but is determined through an indirect effect, which is the acoustic wave generated in the sample due to its thermal expansion. The conversion from optical to thermal energy therefore depends on some physico-thermal properties of the sample (not only from the analysed species, but also and mainly from the buffer gas). Consequently, PAS is not an absolute method and a calibration is essential. Furthermore, molecular relaxation of the excited rovibrational energy into sample heating is a key step in the generation of the PA signal. Whereas this effect can be assumed instantaneous in most cases, since it is much faster than the time scale of the laser modulation, it turns out that this relaxation is much slower in some particular gas mixtures, and the corresponding long relaxation time can strongly influence the generation of the PA signal. Such a phenomenon leads for example to the well-known effect of kinetic cooling of CO<sub>2</sub> observed in the MIR region, which arises when a mixture of CO<sub>2</sub> diluted in N<sub>2</sub> is analysed with a CO<sub>2</sub> laser [6, 7]. In that case, the energy absorbed by the CO<sub>2</sub> molecules results from a hot-band transition, which is rapidly followed by a resonant energy transfer between CO<sub>2</sub> and N<sub>2</sub> vibrational states. As a result of this process, the CO<sub>2</sub> molecules relax in their ground state, where their energy is lower than before the laser-induced transition. This leads to an effective cooling (instead of the usual heating) of the gas sample, which results in a 180 degrees phase lag of the PA signal with respect to the laser modulation. A similar effect has also been recently described in the NIR range, when detecting CO<sub>2</sub> at 1.43 μm using an external-cavity laser diode [8].

The occurrence of such negative molecular relaxation effects in PAS will probably tend to increase in the future for different reasons. Firstly, the number of applications of PAS in the NIR range is currently increasing, thanks to the incomparable properties of DFB lasers and their constantly rising optical power. Some undesirable influences of molecular relaxation are more likely to occur in the NIR than in the MIR, due to the higher vibrational energy levels involved, which results in a more complicated relaxation pathway of the excited molecule and increases the possibilities of vibrational energy transfer to the buffer-gas molecules. Some applications of PAS also concern the monitoring of different gaseous impurities in the control of advanced manufacturing processes. These processes often make use of high-purity gases (such as N<sub>2</sub> or O<sub>2</sub>), in which contaminants have to be monitored at very low levels. The absence of water vapour in these samples increases the influence of relaxation effects, as water usually contributes to favour the relaxation of many species [1]. Finally, additional molecular relaxation effects are expected to occur in a novel alternative technique of PAS, the so-called quartz-enhanced PAS (QE-PAS), which has been recently introduced by Kosterev et al. [9–11]. This method uses a miniature high-*Q* piezoelectric crystal such as found in any watch (a quartz tuning fork) both as a PA cell and as a pressure transducer. This system enables the use of extremely small sample volumes (< 1 mm<sup>3</sup>), but is currently operating only at a much higher resonant frequency (around 32.8 kHz) than traditional PA sensors. Therefore, relaxation effects assume more importance at such a high frequency, as demonstrated in a recent publication [10], due to the slower relaxation rate compared to the modulation frequency. This effect is still amplified by

the fact that QE-PAS is usually performed at reduced pressure (down to 60 Torr [11]) in order to increase the response of the piezoelectric tuning fork, which enhances the influence of relaxation effects.

In this paper, we report a particular example demonstrating the fundamental role played by molecular relaxation in PAS and the dramatic resulting modification of the response of a PA sensor. This example concerns the detection of methane (CH<sub>4</sub>) at trace level in dry oxygen and oxygen–nitrogen mixtures using a PA sensor working with a 1.65-μm DFB laser. Our primary interest for methane-trace monitoring in oxygen was for process control in the manufacturing of the novel low-water-peak fibres developed for optical telecommunications. This new type of fibres, also called metro fibres or zero-water-peak fibres (ZWPFs), is designed to enable optical transmission in the E-band (1360–1460 nm) in order to open up this window for implementing cost-effective coarse wavelength division multiplexing (CWDM) technology for current or future network applications [12]. In standard silica optical fibres, a strong hydroxyl ion (OH<sup>-</sup>) absorption peak, centred at 1390 nm, prevents transmission in the wavelength range extending from roughly 1350 nm to 1480 nm. This peak is often referred to as a water peak, since it is mainly due to the presence of moisture contamination during the manufacturing process of the synthetic silica fibre preform, usually made by modified chemical vapour deposition (MCVD). However, other hydrogenated compounds, such as CH<sub>4</sub> or HCl, present as impurities in the MCVD process, may also contribute to this absorption peak, as they strongly react with the high oxygen concentration used in the process, which leads to the production of OH<sup>-</sup> that is finally trapped in the optical fibre. These chemical reactions are very efficient due to the elevated temperature of the process. A sensitive (sub-part-per-million (sub-ppm) level), continuous and on-line monitoring of these contaminants is therefore required in the ZWPF manufacturing process. Regarding CH<sub>4</sub>, this species needs to be monitored in the presence of a large amount of O<sub>2</sub>, as this substance is mainly used as a carrier gas in the MCVD process. As will be shown later, the methane PA signal is poorly generated in such conditions, which prevents at first glance the realization of a PA sensor for this application. By chance, another carrier gas, helium (He), is also added in large quantities (several tens of percent) to oxygen in the MCVD process and, as will be demonstrated, this substance is highly efficient in promoting the vibrational relaxation of methane–oxygen mixtures, thus making possible CH<sub>4</sub> monitoring by PAS for MCVD process control.

## 2 Influence of molecular relaxation in photoacoustics

PAS basically consists in exciting an absorbing gas sample with a modulated laser beam at a proper wavelength and detecting the generated acoustic wave using a microphone [13]. The acoustic wave occurs as a result of molecular absorption of photons and subsequent deactivation of the excited rovibrational state via inelastic collisions with the neighbouring molecules (collisional relaxation). When the internal energy of the molecule (vibration) is transferred into kinetic energy (translation) of the surrounding molecules, pe-

Reaction	Rate [s <sup>-1</sup> atm <sup>-1</sup> ]	Ref.	Reaction	Rate [s <sup>-1</sup> atm <sup>-1</sup> ]	Ref.
<b>(R<sub>1</sub>)</b> CH <sub>4</sub> <sup>*</sup> ( <i>nv</i> <sub>4</sub> ) + CH <sub>4</sub> → CH <sub>4</sub> <sup>*</sup> (( <i>n</i> - 1) <i>v</i> <sub>4</sub> ) + CH <sub>4</sub> <sup>*</sup> ( <i>v</i> <sub>4</sub> )	2.7 × 10 <sup>8</sup>	[14]	<b>(R<sub>7</sub>)</b> O <sub>2</sub> <sup>*</sup> ( <i>v</i> ) + O <sub>2</sub> → O <sub>2</sub> + O <sub>2</sub>	6.3 × 10 <sup>1</sup>	[16]
<b>(R<sub>2</sub>)</b> CH <sub>4</sub> <sup>*</sup> ( <i>nv</i> <sub>4</sub> ) + CH <sub>4</sub> → CH <sub>4</sub> <sup>*</sup> (( <i>n</i> - 1) <i>v</i> <sub>4</sub> ) + CH <sub>4</sub>	8 × 10 <sup>5</sup>	[14]	<b>(R<sub>8</sub>)</b> O <sub>2</sub> <sup>*</sup> ( <i>v</i> ) + N <sub>2</sub> → O <sub>2</sub> + N <sub>2</sub>	4 × 10 <sup>1</sup>	[16]
<b>(R<sub>3</sub>)</b> CH <sub>4</sub> <sup>*</sup> ( <i>nv</i> <sub>4</sub> ) + O <sub>2</sub> → CH <sub>4</sub> <sup>*</sup> (( <i>n</i> - 1) <i>v</i> <sub>4</sub> ) + O <sub>2</sub> <sup>*</sup> ( <i>v</i> )	~ 3 × 10 <sup>7</sup>		<b>(R<sub>9</sub>)</b> O <sub>2</sub> <sup>*</sup> ( <i>v</i> ) + H <sub>2</sub> O → O <sub>2</sub> + H <sub>2</sub> O	1.1 × 10 <sup>6</sup>	[16]
<b>(R<sub>4</sub>)</b> CH <sub>4</sub> <sup>*</sup> ( <i>nv</i> <sub>4</sub> ) + O <sub>2</sub> → CH <sub>4</sub> <sup>*</sup> (( <i>n</i> - 1) <i>v</i> <sub>4</sub> ) + O <sub>2</sub>	1.3 × 10 <sup>5</sup>	[15]	<b>(R<sub>10</sub>)</b> O <sub>2</sub> <sup>*</sup> ( <i>v</i> ) + CH <sub>4</sub> → O <sub>2</sub> + CH <sub>4</sub> <sup>*</sup> ( <i>v</i> <sub>4</sub> )	2 × 10 <sup>7</sup>	[17]
<b>(R<sub>5</sub>)</b> CH <sub>4</sub> <sup>*</sup> ( <i>nv</i> <sub>4</sub> ) + N <sub>2</sub> → CH <sub>4</sub> <sup>*</sup> (( <i>n</i> - 1) <i>v</i> <sub>4</sub> ) + N <sub>2</sub>	8 × 10 <sup>4</sup>	[14]	<b>(R<sub>11</sub>)</b> O <sub>2</sub> <sup>*</sup> ( <i>v</i> ) + CH <sub>4</sub> → O <sub>2</sub> + CH <sub>4</sub>	1 × 10 <sup>6</sup>	[18]
<b>(R<sub>6</sub>)</b> N <sub>2</sub> <sup>*</sup> ( <i>v</i> ) + N <sub>2</sub> → N <sub>2</sub> + N <sub>2</sub>	1.0	[16]	<b>(R<sub>12</sub>)</b> O <sub>2</sub> <sup>*</sup> ( <i>v</i> ) + He → O <sub>2</sub> + He	2.3 × 10 <sup>4</sup>	[19]

**TABLE 1** Examples of relaxation rates of some vibrational states with different collisional partners. Reactions labelled in **bold** correspond to V-T processes, the others to V-V processes

riodic heating occurs in the sample and induces a pressure wave. In order to efficiently generate this PA signal, the typical time scale of the vibration-to-translation (V-T) energy transfer should be much shorter than the period of the laser modulation, which is generally in the millisecond range for traditional PAS, but may be reduced to 30 μs in the novel QE-PAS technique [9–11]. This requirement is most often fulfilled in standard PAS, since the collisional relaxation time of most molecules ranges from nanoseconds to hundreds of microseconds at atmospheric pressure. However, the relaxation time of some particular molecules may be orders of magnitude longer [14–19]. In particular, this is the case for a few diatomic molecules, such as N<sub>2</sub> or O<sub>2</sub> (see Table 1), and for collisions with some particular partners (N<sub>2</sub> and O<sub>2</sub>, too). Therefore, heat release may be delayed in a gas mixture if the excess energy of the excited molecules can be channelled by collisions, through vibration-to-vibration (V-V) energy transfers, to a long-lifetime excited state of the surrounding molecules. As a result, the PA signal is severely damped when the time scale of the V-T processes is comparable to or longer than one period of the laser modulation. The dependence of the PA signal with respect to the molecular relaxation time  $\tau$  is given by [1]

$$S_{\text{PA}} = \frac{C_{\text{cell}} C \alpha P_0}{\sqrt{1 + (\omega\tau)^2}}, \quad (1)$$

where  $C_{\text{cell}}$  is the cell constant (in [V cm/W]),  $C$  the gas concentration,  $\alpha$  the absorption coefficient,  $P_0$  the incident optical power and  $\omega = 2\pi f$  the modulation angular frequency.

The phase of the PA signal is given by  $\tan \varphi = -\omega\tau$ . When the relaxation process is fast enough (which corresponds to most cases encountered in PAS), the condition  $\omega\tau \ll 1$  is fulfilled. Therefore, the PA signal becomes independent of the relaxation time ( $S_{\text{PA}} = C_{\text{cell}} C \alpha P_0$ ) and is in phase with the laser modulation ( $\varphi = 0$ ). However, the situation is drastically different when the relaxation process is slow. In that case ( $\omega\tau \gg 1$ ), the PA signal is phase shifted with respect to the laser modulation ( $\varphi \neq 0$ ) and becomes directly linear with the relaxation rate:

$$S_{\text{PA}} \cong C_{\text{cell}} C \frac{\alpha P_0}{\omega} \tau^{-1}. \quad (2)$$

In a gas mixture, the relaxation rate of an excited state of a molecule  $M$  is given by a weighted sum of the relaxation rates corresponding to collisions with the different types of surrounding molecules  $M_i$  and taking into account the concentration  $C_i$  of each species:

$$\tau_M^{-1} = \sum_i C_i \tau_{M-M_i}^{-1}. \quad (3)$$

### 3 Experimental details

A fibre-coupled PA sensor has been developed for CH<sub>4</sub> detection. The experimental setup is shown in Fig. 1. A PA cell has been optimized for high sensitivity and good immunity to environmental noise [20]. The cell is made of a central stainless steel tube, 17-cm long with 6-mm inner

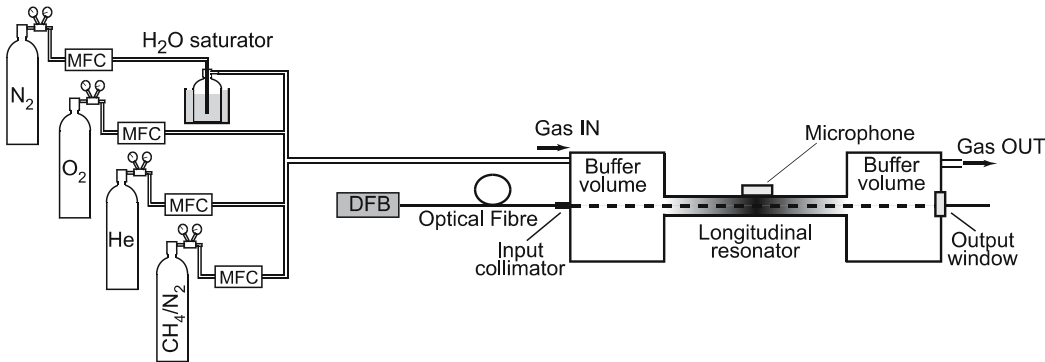


**FIGURE 1** Scheme of the experimental set-up, including the PA sensor and a gas-mixing system made of four mass-flow controllers (MFCs) to generate different CH<sub>4</sub> concentrations and carrier-gas compositions. Light from a current-modulated 1651-nm DFB laser is launched into the acoustic resonator through a fibre collimator and the generated PA signal is detected in the centre of the resonator using an electret microphone

diameter, acting as an acoustic resonator, and two external larger volumes, acting as acoustic filters. The resonator was operated in its first longitudinal mode, at a resonance frequency roughly equal to 1 kHz in air. The length of the buffer volumes was adjusted to a quarter of the acoustic wavelength, in order to minimize the coupling of acoustic noise (ambient noise, windows' noise) into the resonator. The acoustic signal was detected in the centre of the resonator, at the maximum of the acoustic standing wave, using a sensitive electret microphone (Knowles EK3032). After amplification, the PA signal was measured using a lock-in amplifier (EG&G 5210) with a time constant usually set to 3 or 10 s. Both the amplitude and the phase of the signal were finally recorded by a computer.

A pigtailed DFB laser (NEL NLK1U5E1AA) was used as a PA excitation source. The laser covered the spectral range 1648–1652 nm when its temperature was changed from 5 °C to 40 °C. The temperature- and current-tuning coefficients were  $-12.3 \text{ GHz}/^\circ\text{C}$  and  $-0.56 \text{ GHz}/\text{mA}$ , respectively. The average laser power at the fibre output was 8 mW in our experimental conditions. The laser was connected to a fibre collimator directly mounted on the outer flange of the buffer volume of the PA cell. The collimated laser beam was properly aligned to the axis of the acoustic resonator, in order to avoid acoustic noise induced by a contact between the tube and the wings of the laser-beam distribution (wall noise). The laser was tuned to the strongest attainable  $\text{CH}_4$  absorption feature at 1650.96 nm (composed of four overlapping lines of the R(4) quadruplet in the  $2\nu_3$  band) and the injection current was modulated at the first longitudinal resonance frequency of the central tube, in order to efficiently excite the PA signal. An enhancement factor  $Q \cong 21\text{--}23$  (depending on the precise buffer-gas composition) was achieved at ambient atmospheric pressure thanks to this resonant configuration.

Semiconductor lasers can be modulated either in intensity (on-off modulation with square waveform) or in wavelength (sine or square modulation of reduced amplitude in order to tune the laser on-line and off-line). In our case, wavelength modulation (WM) can produce a slightly higher (25%) PA signal than intensity modulation (IM) when an optimal modulation depth is used [21]. However, a WM-induced PA signal is more sensitive to the width of the absorption feature than in the case of IM, since WM signals directly depend on the ratio of the modulation depth to the absorption line width (a maximum signal is obtained when the modulation depth is roughly twice the line width [22]). Different buffer gases ( $\text{N}_2/\text{O}_2$  mixtures of different compositions, adjunction of several percent of water vapour or helium) have been used in our experiments in order to study the influence of molecular relaxation on the PA signal. Since the foreign-broadening coefficient of the  $\text{CH}_4$  absorption feature of interest changes with the composition of the carrier gas [23], IM has been preferred since it is less dependent on the width of the absorption feature than WM. For this purpose, the laser current was square modulated between threshold and a value close to the current limit, in order to achieve complete IM (IM index  $M = 1$ ). However, pure IM was not achieved in these conditions, since residual WM also occurred as a result of the laser chirp induced by the current pulses. But, since measurements were performed at atmospheric pressure where the  $\text{CH}_4$  absorption feature is several GHz wide, the effect of the residual WM was very weak

compared to IM (i.e. the laser chirp was much smaller than the width of the absorption feature) and its influence on the PA signal could be neglected. This has been confirmed by experimental measurements of the PA spectrum of methane that showed no significant line broadening.

Various  $\text{CH}_4$  concentrations and carrier-gas compositions have been prepared from certified cylinders using a multi-gas controlling unit (MKS 647C) and mass-flow controllers (MKS 1179). Two cylinders of  $\text{CH}_4$  buffered in nitrogen (5000 ppm and 100 ppm) and three pure gases ( $\text{N}_2$ ,  $\text{O}_2$  and He) have been used. With four different mass-flow controllers ( $2 \times 100 \text{ sccm}$ ,  $1 \times 500 \text{ sccm}$  and  $1 \times 1000 \text{ sccm}$ ),  $\text{CH}_4$  concentrations ranging from 5000 ppm down to 0.4 ppm could be generated when  $\text{N}_2$  was used as the carrier gas, and from 2000 ppm down to 0.4 ppm in  $\text{N}_2/\text{O}_2$  mixtures (with a precision on the  $\text{CH}_4$  concentration that was dependent on the dilution factor, but always better than 10%). The flow rates in the mass-flow controllers were always adjusted in order to have a total gas flow of 500 sccm in the PA cell. Such a flow rate enables a fast enough response time to changing concentrations without inducing additional acoustic noise. The water-vapour content in the gas mixture could also be adjusted by passing part of the flow through a saturator, i.e. a water-filled glass cuvette placed in a thermostat bath. The flow exiting the cuvette was saturated in water vapour and the humidity was dependent only on the bath temperature. The humidification of the gas sample was important to study the influence of molecular relaxation effects, as water vapour is usually an efficient catalyst that enhances the vibrational relaxation rate of many species.

With the experimental setup previously described, methane diluted in dry  $\text{N}_2$  has been first measured. In that case, a detection limit of 0.18 ppm (defined for a signal-to-noise ratio  $\text{SNR} = 3$  and with 10-s integration time) has been achieved. Then,  $\text{CH}_4$  was diluted in oxygen in order to investigate the sensitivity of the PA system for our application of interest, i.e. the monitoring of  $\text{CH}_4$  in the MCVD process. The PA signal detected in these conditions was more than one order of magnitude lower than in pure  $\text{N}_2$ , and almost no signal could be measured below 10 ppm of  $\text{CH}_4$ . After identifying that this behaviour resulted from molecular relaxation, we decided to investigate this phenomenon in more detail and to study PA methane monitoring in different  $\text{N}_2/\text{O}_2$  mixtures, as well as the effect of various catalysts ( $\text{H}_2\text{O}$ , He) that may promote the vibrational relaxation of the  $\text{CH}_4\text{--O}_2$  system. As relaxation effects strongly depend on the frequency of the excited acoustic wave, different resonances of our PA cell have been considered in this experimental study. The three first longitudinal modes of odd order – labelled (001), (003) and (005) – have been used, with typical resonance frequencies in air of 1 kHz, 3 kHz and 5 kHz (the even longitudinal modes cannot be used, as they are not excited by the laser beam in this geometry due to symmetry reasons).

## 4 Results and discussion

### 4.1 First experimental evidence of relaxation effects in the $\text{CH}_4\text{--O}_2$ system

The variation of the PA response corresponding to 100 ppm of  $\text{CH}_4$  in different dry  $\text{N}_2/\text{O}_2$  mixtures is shown in Fig. 2. For this measurement, the complete acoustic reson-

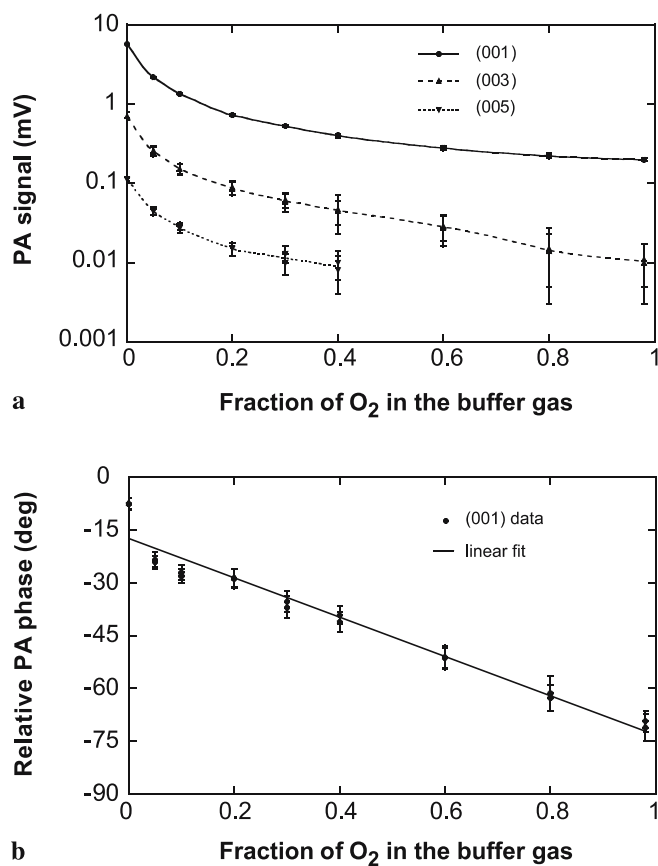


**FIGURE 2** Variation of the PA response corresponding to 100 ppm CH<sub>4</sub> as a function of the O<sub>2</sub> fraction in N<sub>2</sub> in the buffer gas. **(a)** PA amplitude of the first three odd-order longitudinal resonances of the PA cell, labelled (001), (003) and (005). **(b)** Phase of the PA signal measured at the first longitudinal resonance; the *solid line* represents a linear fit of the data. *Error bars* shown on the experimental data correspond to the standard deviation of the fitting process used to determine the parameters of the acoustic resonance. Two different measurements are displayed for each experimental condition

ance (amplitude and phase) has been recorded by scanning the laser modulation frequency. The phase measurements do not represent absolute values, as some additional electronic phase shifts may be present even in the absence of molecular relaxation effects. However, the reference phase of the lock-in detection was kept fixed during all the measurements, so that relative phase variations may be attributed to relaxation effects. The parameters of the resonance (amplitude, central frequency and phase,  $Q$  factor) have been extracted from a fitting procedure of the experimental data and the level of uncertainty of each parameter has been determined from the standard deviation of the fitting process. The PA energy (square of the PA amplitude) was fitted by a Lorentzian distribution in order to determine the centre, amplitude and  $Q$  factor of the resonance. The  $Q$  factor is given by the ratio between the centre frequency and the width (half-width at half maximum) of the Lorentzian distribution of the acoustic energy. The phase data were fitted by a fifth-order polynomial and the value at the centre of the resonance (given by the Lorentzian fit) was determined. From these measurements, it turned out that the  $Q$  factor was only marginally modified between measurements in pure N<sub>2</sub> and O<sub>2</sub> (for example, it was reduced from  $Q \cong 23$  in pure N<sub>2</sub> to  $Q \cong 21$

in O<sub>2</sub> for the first longitudinal mode). The PA amplitude in Fig. 2a is reduced by more than one order of magnitude when measured in O<sub>2</sub> in comparison to the case of pure N<sub>2</sub>, and the signal is strongly reduced in N<sub>2</sub>/O<sub>2</sub> mixtures containing only a few percent of O<sub>2</sub>. The behaviour is similar for the three considered modulation frequencies (1 kHz, 3 kHz and 5 kHz), but the data are less accurate at higher frequency due to a severe reduction in the signal-to-noise ratio, which results from the combination of the  $1/f$  dependence of the PA effect and the decrease of the overlap integral between the laser beam and high-order acoustic modes. The phase variation of the PA signal is also shown in Fig. 2b for the first longitudinal mode. A linear change is observed when increasing the O<sub>2</sub> concentration. The strong reduction of the PA signal observed when switching from pure N<sub>2</sub> to O<sub>2</sub> as a carrier gas and the associated phase variation are induced by particular molecular relaxation effects occurring in the CH<sub>4</sub>-O<sub>2</sub> system (discussed in Sect. 4.2) and are hardly influenced by the  $Q$  factor of the resonance or by other physical parameters of the buffer gas.

#### 4.2 Discussion of the relaxation of CH<sub>4</sub> in O<sub>2</sub>

The unexpected experimental results reported in Fig. 2 about the monitoring of methane in oxygen by PAS are related to singular molecular relaxation effects occurring in the CH<sub>4</sub>-O<sub>2</sub> system. They may be explained by considering the deactivation pathway followed by the CH<sub>4</sub> molecules excited by the laser radiation. A complete description of the spectroscopic properties of CH<sub>4</sub> is given in Ref. [15] and the rovibrational energy transfer processes in CH<sub>4</sub>-N<sub>2</sub>/O<sub>2</sub> mixtures are also discussed in a series of papers [15, 16, 24]. We just recall here the main spectroscopic characteristics of CH<sub>4</sub> molecules that are essential for the understanding of our experimental results.

The CH<sub>4</sub> molecule has four vibrational modes: two bending vibrations  $\nu_2$  (asymmetric) and  $\nu_4$  (symmetric), and two stretching vibrations  $\nu_1$  (symmetric) and  $\nu_3$  (asymmetric). The first excited bending levels  $\nu_2$  and  $\nu_4$  are located at 1533 and 1311 cm<sup>-1</sup> and the stretching levels  $\nu_1$  and  $\nu_3$  at 2917 and 3019 cm<sup>-1</sup>, approximately two times higher in frequency than the two former ones. Consequently, the vibrational energies of methane can be viewed as clusters (called polyads) of states interacting together through Fermi or Coriolis resonances, as shown in Fig. 3. The spacing between two successive polyads is about 1500 cm<sup>-1</sup>. Due to the strong interactions existing between the states in a given polyad, the spectroscopic analysis of any vibrational state needs to take into account simultaneously all the states of the polyad to which the level belongs [15]. This characteristic is important for the understanding of the collisional relaxation of methane. In particular, very fast energy transfers (in the nanosecond range) occur between the states of the same polyad (intermodal transfer) for both CH<sub>4</sub>-CH<sub>4</sub> and CH<sub>4</sub>-O<sub>2</sub> collisions. Therefore, the energy transfer between two polyads essentially occurs via the exchange of one  $\nu_4$  vibrational quantum (see reactions  $R_1$  and  $R_3$  in Table 1), since this is the smallest energy quantum. For CH<sub>4</sub>-O<sub>2</sub> collisions, the de-excitation of the CH<sub>4</sub> molecule is accompanied by a resonant excitation of the first vibrational state of oxygen, O<sub>2</sub><sup>\*</sup>( $\nu$ ), due to its proximity with the

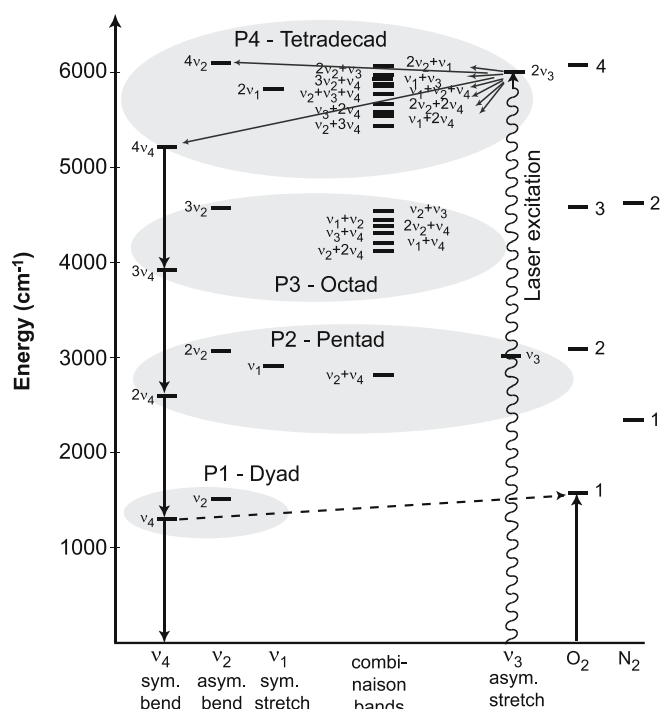


**FIGURE 3** Energy-level diagram of  $\text{CH}_4$  molecule, showing the laser excitation to the  $2\nu_3$  state and the subsequent relaxation scheme with the resonant coupling between  $\text{CH}_4^*$  ( $\nu_4$ ) and  $\text{O}_2^*$  ( $\nu$ ) levels (dashed arrow)

$\text{CH}_4^*$  ( $\nu_4$ ) level. For weak  $\text{CH}_4$  concentrations, the transfer to the lower polyads occurs predominantly via the resonant process  $R_3$  and, at each relaxation step, the energy released by  $\text{CH}_4$  is transferred to oxygen molecules. As a result, the whole 1.65- $\mu\text{m}$  laser energy initially absorbed in the  $\text{CH}_4^*$  ( $2\nu_3$ ) state finally accumulates in the  $\text{O}_2^*$  ( $\nu$ ) vibrational state of oxygen. According to Table 1, the relaxation time of this state at atmospheric pressure ( $\tau_{\text{O}_2-\text{O}_2} = 1/63$  [s]) is much longer than one period of the laser modulation (around 1 ms for 1-kHz modulation frequency), so that no PA signal is coherently generated with the laser modulation. This explains the very small PA signal observed when measuring  $\text{CH}_4$  in  $\text{O}_2$ . The situation is totally different for  $\text{CH}_4$  diluted in  $\text{N}_2$ , as the first vibrational state of  $\text{N}_2$  has a larger energy than the  $\text{CH}_4^*$  ( $\nu_4$ ) level, so that no efficient V-V transfer can occur.

In the different  $\text{N}_2/\text{O}_2$  mixtures considered in Fig. 2, two different relaxation pathways may be followed by the  $\text{CH}_4$  excited molecules. The first involves  $\text{CH}_4\text{-N}_2$  collisions that result in the V-T process (reaction  $R_5$ ) that generates a PA signal at all considered modulation frequencies. The second involves  $\text{CH}_4\text{-O}_2$  collisions that result in the resonant V-V transfer (reaction  $R_3$ ) and in an accumulation of the energy in the  $\text{O}_2^*$  ( $\nu$ ) excited state.  $\text{CH}_4\text{-CH}_4$  collisions may be neglected here since the considered  $\text{CH}_4$  concentration is several orders of magnitude smaller than  $\text{N}_2$  and  $\text{O}_2$  concentrations. In the second relaxation pathway ( $\text{CH}_4\text{-O}_2$  collisions), the transfer into kinetic energy is limited by the long relaxation time of the excited  $\text{O}_2^*$  ( $\nu$ ) state for both  $\text{O}_2\text{-N}_2$  and  $\text{O}_2\text{-O}_2$  collisions according to reactions  $R_7$  and  $R_8$  in Table 1. A very high value of the parameter  $\omega\tau$  is obtained in this case for each resonance ( $\omega\tau \cong 100, 300$  and  $500$  for modes (001), (003) and (005), respectively). According to Eq. (1), it im-

plies that this energy is almost entirely lost for the generation of the PA signal for our three resonances and only the energy relaxed through  $\text{CH}_4\text{-N}_2$  collisions contributes to the PA signal. When the  $\text{O}_2$  concentration is raised, the amount of energy transferred to  $\text{O}_2$  rapidly increases and the PA signal is reduced accordingly, which qualitatively explains the behaviour observed in Fig. 2a. The fact that only the V-T process induced by  $\text{CH}_4\text{-N}_2$  collisions contributes to the PA signal explains the similar behaviour observed for the three considered frequencies. In addition, the phase of the PA signal is also affected when increasing the  $\text{O}_2$  concentration, since the relaxation time corresponding to  $\text{CH}_4\text{-N}_2$  collisions depends on the  $\text{N}_2$  concentration according to Eq. (3). This leads to a linear variation of the phase as qualitatively observed in Fig. 2b. However, the experimental behaviour cannot be quantitatively explained by the relaxation rates of the processes presented in Table 1. This may result from some inaccuracies in the published data used for the evaluation of the relaxation rates or from the possibility that other processes also contribute to the relaxation.

Due to the strong and very fast coupling between  $\text{CH}_4^*$  ( $\nu_4$ ) and  $\text{O}_2^*$  ( $\nu$ ) states, the negative influence of oxygen on the generation of the methane PA signal is already significant even for small  $\text{O}_2$  concentrations (some percent) in the carrier gas. Therefore, such a situation may even be encountered when monitoring  $\text{CH}_4$  in ambient air (21%  $\text{O}_2$ ) in relatively dry conditions. In addition, this effect is due to the resonant coupling between the lower  $\text{CH}_4$  energy level ( $\nu_4$ ) and the first vibrational mode of  $\text{O}_2$  as described herein. It is therefore independent of the upper level of the molecular transition excited by the laser radiation. This has been confirmed by measurements performed in the 2.37- $\mu\text{m}$  range ( $\nu_1 + \nu_4$  band belonging to the lower polyad P3) using a new type of GaSb-based semiconductor DFB laser [25]. It may be noticed in Fig. 4 that the reduction of the PA signal observed when increasing the  $\text{O}_2$  concentration in the carrier gas is comparable

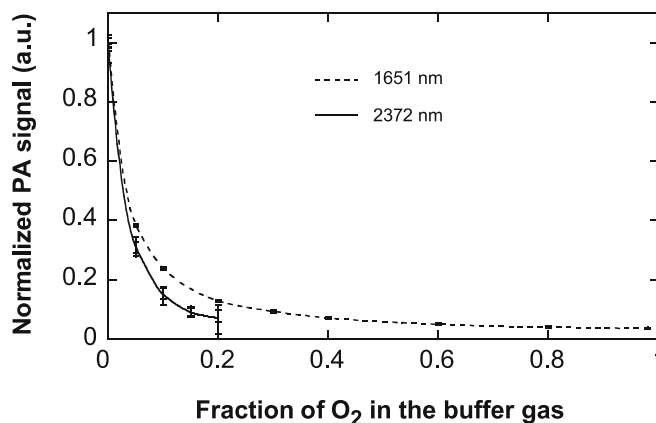


**FIGURE 4** Variation of the PA signal (amplitude of the first longitudinal resonance) as a function of the  $\text{O}_2$  concentration in the buffer gas for two different excited  $\text{CH}_4$  transitions:  $2\nu_3$  in polyad P4 ( $\lambda = 1651$  nm) and  $\nu_1 + \nu_4$  in polyad P3 ( $\lambda = 2372$  nm). A  $\text{CH}_4$  concentration of 100 ppm was considered and the PA signals were normalized at each wavelength to the value obtained in pure  $\text{N}_2$ . Error bars shown on the experimental data correspond to the standard deviation of the fitting process used to determine the parameters of the acoustic resonance

between the 1.65- $\mu\text{m}$  and the 2.37- $\mu\text{m}$  absorption bands (it is even slightly more important at 2.37  $\mu\text{m}$ ).

A similar behaviour has already been reported for the detection of  $\text{CH}_4$  in  $\text{O}_2/\text{N}_2$  mixtures in the fundamental  $\nu_4$  vibrational band [26]. In that case, a 150 degrees phase lag of the PA signal was observed and this phenomenon was considered as a kinetic cooling effect, due to its similarity with the  $\text{CO}_2$  kinetic cooling. The behaviour reported here for the  $\text{CH}_4$ - $\text{O}_2$  system is also induced by molecular relaxation effects, but some experimental evidence shows that it is distinct from a kinetic cooling. Firstly, the  $\text{CH}_4$  transition of interest ( $2\nu_3$  or  $\nu_1 + \nu_4$ ) does not belong to a hot band, opposite to the kinetic cooling of  $\text{CO}_2$ . Furthermore, the observed phase shift of the PA signal is very far from the theoretical value of 180 degrees achieved in the case of kinetic cooling. Molecular relaxation effects in the  $\text{CH}_4$ - $\text{O}_2$  mixture are responsible for a delay in the PA signal generation, but no effective cooling occurs.

### 4.3 Parabolic response of the sensor with respect to $\text{CH}_4$ concentration

The response of the PA sensor to varying methane concentrations is shown in Fig. 5 for different buffer-gas compositions: pure  $\text{N}_2$ , 60%  $\text{O}_2/40\%$   $\text{N}_2$  dry and humidified with 0.15% or 1.1% of water vapour (absolute humidity). For these measurements, both the amplitude and the phase of the PA signal have been continuously recorded at the centre of the first resonance during 5 min. The average value and the standard deviation of the data have been determined in each case. A mixture containing 60% of  $\text{O}_2$  and 40% of  $\text{N}_2$  was chosen for the following reasons: (i) in order to be not influenced by other undesirable parameters (variation of the resonance frequency, broadening of the absorption line, etc.), it was chosen to keep always the same mixing ratio between  $\text{N}_2$  and  $\text{O}_2$  for all considered  $\text{CH}_4$  concentrations; (ii) as our certified cylinders were buffered in  $\text{N}_2$ , it was not possible to dilute methane in pure  $\text{O}_2$ ; with only 60% of  $\text{O}_2$ , a wide variety of methane concentrations could be achieved, ranging from 2000 ppm down to 0.4 ppm; (iii) molecular relaxation effects already have a strong influence in a mixture containing 60% of  $\text{O}_2$  as shown in Fig. 2.

We observe in Fig. 5 a similar response of the sensor when either pure  $\text{N}_2$  or a  $\text{O}_2/\text{N}_2$  mixture with a high  $\text{H}_2\text{O}$  content (1.1% absolute humidity) is considered. In both cases, a very good linearity ( $R > 0.99$ ) is obtained over more than four orders of magnitude of concentration. The phase of the PA signal also remains constant over the full range of  $\text{CH}_4$  concentrations. The  $\text{CH}_4$  level resulting in a noise-equivalent signal was found to be 60 ppb for the first longitudinal resonance (for 10-s integration time). The measured signal was even slightly higher in the humidified  $\text{O}_2/\text{N}_2$  mixture than in pure  $\text{N}_2$ , which may suggest that a very small influence of relaxation effects even occurs in pure  $\text{N}_2$ . This assumption seems to be confirmed by the small phase difference observed between these two carrier gases. This point is not discussed in this paper, but will be addressed in a future publication. A strongly different behaviour was observed when a dry or weakly humidified (0.15% absolute humidity)  $\text{O}_2/\text{N}_2$  mixture was used as a carrier gas. In these cases, the PA signal was

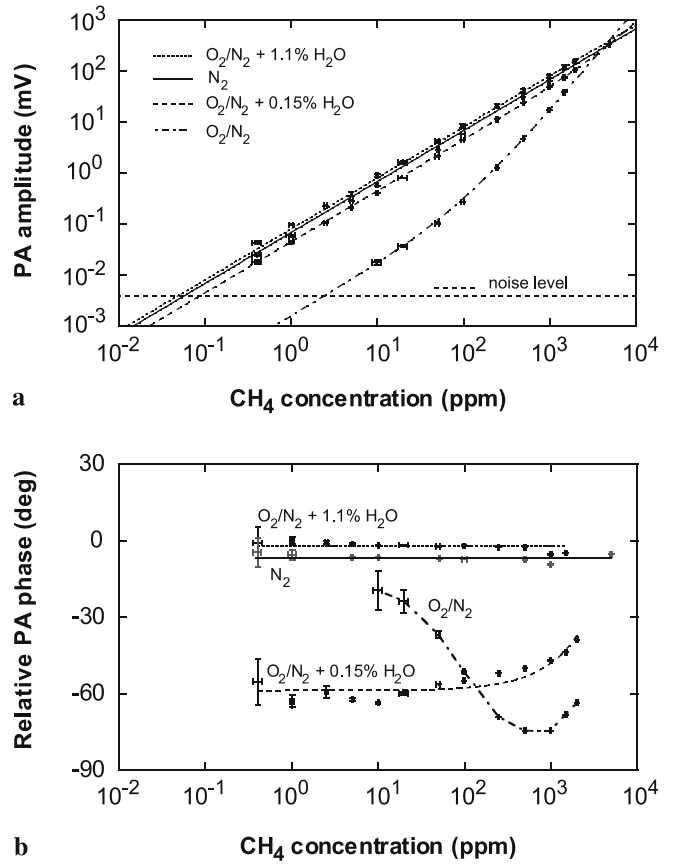


**FIGURE 5** Amplitude (a) and phase (b) variation of the PA signal measured at the first longitudinal resonance as a function of the  $\text{CH}_4$  concentration for different carrier gases: pure  $\text{N}_2$ , dry 60%  $\text{O}_2/40\%$   $\text{N}_2$ , 60%  $\text{O}_2/40\%$   $\text{N}_2$  humidified with 0.15% and 1.1%  $\text{H}_2\text{O}$  (absolute humidity). Error bars shown on the plot correspond to the uncertainty on the  $\text{CH}_4$  concentration generated with the MFCs (*horizontal axis*) and to the standard deviation of the PA signal recorded in a 5-min period (*vertical axis*). Lines in (a) are the result of a fit by a linear function (for pure  $\text{N}_2$  and  $\text{O}_2/\text{N}_2$  with 1.1%  $\text{H}_2\text{O}$ ) or by the sum of a linear and a quadratic term (for dry  $\text{O}_2/\text{N}_2$  and  $\text{O}_2/\text{N}_2$  with 0.15%  $\text{H}_2\text{O}$ ). In (b), lines correspond to a constant phase for  $\text{N}_2$  and  $\text{O}_2/\text{N}_2$  with 1.1%  $\text{H}_2\text{O}$  and to a linear fit for  $\text{O}_2/\text{N}_2$  with 0.15%  $\text{H}_2\text{O}$ . For the dry  $\text{O}_2/\text{N}_2$  mixture, the line is just an interpolation between the experimental points

no longer linear, but was expressed as the sum of a linear and a quadratic term (clearly visible for the dry  $\text{O}_2/\text{N}_2$  mixture). The  $\text{CH}_4$  concentration resulting in a noise-equivalent signal was depreciated to 2.5 ppm in dry  $\text{O}_2/\text{N}_2$  (for 10-s integration time). The phase of the PA signal is also changing as a function of the  $\text{CH}_4$  concentration, and the phase variations are larger for the dry  $\text{O}_2/\text{N}_2$  mixture.

The parabolic response with respect to the  $\text{CH}_4$  concentration observed in the presence of  $\text{O}_2$  is also a clear indication of the importance of relaxation effects in the  $\text{CH}_4$ - $\text{O}_2$  system. Whereas the collisional V-T relaxation of  $\text{O}_2^*$  ( $\nu$ ) is very slow for  $\text{O}_2$ - $\text{O}_2$  collisions, it is more than four orders of magnitude faster for  $\text{O}_2$ - $\text{CH}_4$  collisions (see reaction  $R_{11}$  in Table 1). So, even for small  $\text{CH}_4$  concentrations, the relaxation time of the  $\text{O}_2^*$  ( $\nu$ ) state is reduced when increasing the  $\text{CH}_4$  concentration. According to Eq. (3), a linear variation of the relaxation rate is obtained for small  $\text{CH}_4$  concentrations:

$$\tau_{\text{O}_2}^{-1} \cong \tau_{\text{O}_2-\text{O}_2}^{-1} + C_{\text{CH}_4} \tau_{\text{O}_2-\text{CH}_4}^{-1} \quad (4)$$

By combining Eqs. (2) and (4), the dependence of the PA signal finally appears as the sum of a linear and a quadratic term, which fully explains the experimental observations:

$$S_{\text{PA}} \cong C_{\text{cell}} C_{\text{CH}_4} \frac{\alpha P_0}{\omega} \left( \tau_{\text{O}_2-\text{O}_2}^{-1} + C_{\text{CH}_4} \tau_{\text{O}_2-\text{CH}_4}^{-1} \right). \quad (5)$$

Therefore, the experimentally observed parabolic response results from a double-linear dependence of the PA signal on the  $\text{CH}_4$  concentration. The first is the usual linear variation with the gas concentration, due to the increasing amount of energy absorbed in the sample. The second is directly induced by the variation of the molecular relaxation rate with the  $\text{CH}_4$  concentration as described by Eq. (4).

The phase variation of the PA signal observed in dry or weakly humidified (0.15%  $\text{H}_2\text{O}$ )  $\text{O}_2/\text{N}_2$  mixtures is more difficult to quantitatively explain. However, a qualitative interpretation may be given based on the previous argument about V–T transfers in a  $\text{CH}_4/\text{N}_2/\text{O}_2$  mixture. The phase evolution observed in the dry  $\text{O}_2/\text{N}_2$  mixture may be qualitatively explained by the characteristics of the relaxation scheme occurring in different ranges of concentration. For low  $\text{CH}_4$  concentration, the energy transferred to  $\text{O}_2^*(\nu)$  via the resonant process  $R_3$  is lost for the PA signal due to the long-lifetime relaxation of  $\text{O}_2^*(\nu)$ . In that case, only the V–T process due to  $\text{CH}_4\text{--N}_2$  collisions (reaction  $R_5$ ) contributes to the PA signal and the phase of this signal is expected to tend to 0 degrees, which seems to correspond to the tendency of the experimental curve at low  $\text{CH}_4$  concentration. On the other hand, the  $\text{O}_2^*(\nu)$  V–T relaxation is strongly hastened at high  $\text{CH}_4$  concentration (reaction  $R_{11}$ ) and becomes comparable to or faster than one period of the laser modulation. Therefore, the energy transferred to  $\text{O}_2^*(\nu)$  partially contributes to the PA signal and the phase tends again to 0 degrees when the  $\text{O}_2^*(\nu)$  relaxation is fast enough, i.e. at high  $\text{CH}_4$  concentration. In the intermediate range of concentration, the two above-mentioned relaxation pathways contribute to the PA signal, with their own amplitude and phase depending on the  $\text{CH}_4$  concentration. In particular, the contribution of  $\text{O}_2\text{--CH}_4$  collisions leads to a phase shift since the factor  $\omega\tau$  is non-negligible in the intermediate range of concentration ( $\omega\tau \cong 1$ ).

When a small quantity of water vapour (0.15% as in Fig. 5) is added to the sample, the relaxation of  $\text{O}_2^*(\nu)$  is promoted and, even at very low  $\text{CH}_4$  concentration, the energy transferred to  $\text{O}_2^*(\nu)$  slightly contributes to the PA signal. This contribution increases with  $\text{CH}_4$  concentration due to the associated reduction of the relaxation time (see Eq. (4)). In this case, the phase of the PA signal changes monotonically with the  $\text{CH}_4$  concentration as observed in Fig. 5b.

If the above qualitative arguments enable us to explain the observed experimental results, a more detailed analysis reveals a large deviation of the measured values from the data calculated by the relaxation rates given in Table 1. This discrepancy may result from some erroneous values indicated in Table 1, but it may also indicate that the relatively simple relaxation scheme we have considered is incomplete and that other processes may contribute to the relaxation, or that other physical processes may play a role in the generation of the PA signal.

#### 4.4 Enhancement of the V–T process rate in $\text{CH}_4\text{--O}_2$ mixtures using a catalyst

Not only is  $\text{CH}_4$  efficient in promoting the V–T relaxation of  $\text{O}_2^*(\nu)$ , but some other species may also act as a catalyst for this relaxation. For example, water vapour is known to promote the vibrational relaxation of several species, including  $\text{O}_2$  (see reaction  $R_9$  in Table 1). This is confirmed by the experimental results shown in Fig. 6, where the variation of the PA signal (amplitude and phase) corresponding to 20 ppm of  $\text{CH}_4$  is displayed as a function of the water content in the 60%  $\text{O}_2/40\%$   $\text{N}_2$  carrier gas. For these measurements, both the amplitude and the phase of the PA signal have been recorded at the centre of the three resonances during 5 min and the average value and the standard deviation of the data have been determined. A constant signal amplitude is obtained for water-vapour contents higher than 1% (absolute humidity), but a strong reduction of the signal is observed below 1% humidity. Furthermore, measurements performed using different acoustic resonances have shown that the decrease of the PA signal occurs at larger  $\text{H}_2\text{O}$  concentrations for higher frequencies. A similar behaviour is observed for the phase of the PA signal. All these observations qualitatively demonstrate the catalytic effect of water vapour for the relaxation of  $\text{O}_2^*(\nu)$ . However, here again the dependence of the PA signal am-

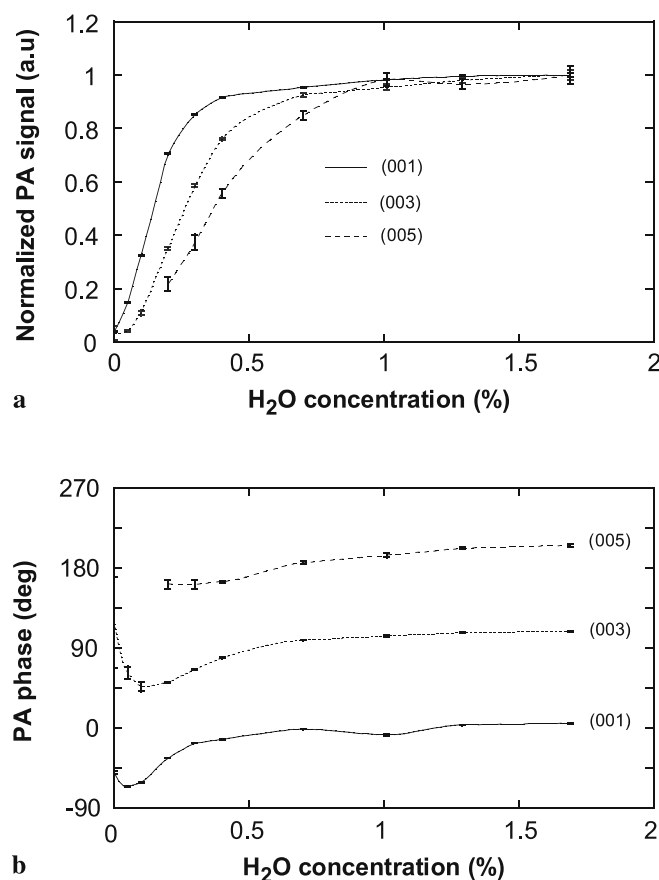


**FIGURE 6** Amplitude (a) and phase (b) dependence of the PA signal corresponding to 20 ppm of  $\text{CH}_4$  as a function of the  $\text{H}_2\text{O}$  content in the carrier gas (composed of 60%  $\text{O}_2$  and 40%  $\text{N}_2$ ) for the three acoustic resonances. Error bars shown on the plot correspond to the standard deviation of the PA signal recorded in a 5-min period



plitude on water concentration disagrees with the values calculated using the data of Table 1. For example, the relaxation rate  $\tau^{-1}$  may be estimated from the point where the normalized PA amplitude in Fig. 5 reaches the value  $1/\sqrt{2}$ , which corresponds to  $\omega\tau = 1$  according to Eq. (1). With the processes considered for the relaxation of  $O_2^*(\nu)$  and the values of Table 1, the calculated relaxation rates for resonances (001), (003) and (005) are about 2.5 times smaller than the measured ones. This discrepancy prevents the development of a precise quantitative description of the relaxation of the considered system based on the relatively simple relaxation scheme that has been proposed and using typical relaxation rates previously published in the literature.

Another species that has been demonstrated to efficiently promote the vibrational relaxation of  $O_2$  is helium (see reaction  $R_{12}$  in Table 1). This is of great importance for our application ( $CH_4$  monitoring in the manufacturing of ZWPFs), as helium is used in large quantities (several tens of percent) in this process. The beneficial influence of helium as a catalyst for the V–T relaxation of  $O_2^*(\nu)$  in the generation of the PA signal is illustrated in Fig. 7. The amplitude of the PA signal is displayed as a function of  $CH_4$  concentration in four different carrier gases:  $N_2$ ,  $O_2$ , He and a mixture of 90%  $O_2$  and 10% He. Except for  $N_2$ , the results displayed in Fig. 7 were not achieved with pure carrier gases. Since our  $CH_4$  certified cylinders were buffered in nitrogen, a residual of  $N_2$  was always present in the gas mixtures considered in Fig. 7. However, this  $N_2$  residual was smaller than 2% for  $CH_4$  concentrations below 100 ppm and its influence on the experimental results is estimated to be of minor importance, so that it can be neglected. The signal measured in He is lower than in  $N_2$  due mainly to the much higher resonance frequency (around 2.5 kHz) induced by the faster acoustic velocity in He and to the smaller quality factor of the resonance that results from the difference in some other physico-thermal constants of the gas, such as density, viscosity and thermal conductivity. But, the difference observed between  $N_2$  and He is not at all related to

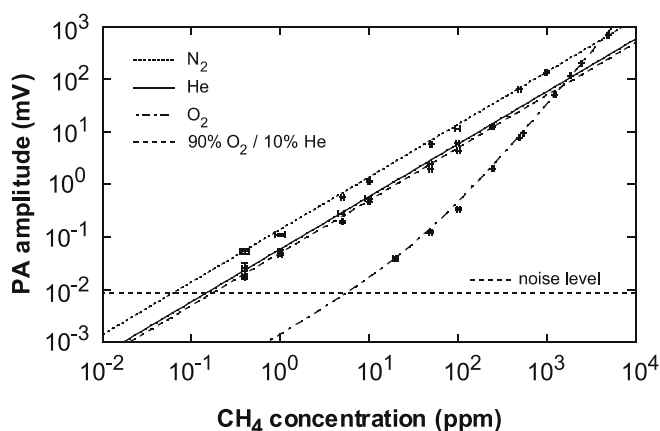


**FIGURE 7** Variation of the PA signal corresponding to the first longitudinal resonance as a function of the  $CH_4$  concentration for different carrier gases ( $N_2$ ,  $O_2$ , He and 90%  $O_2$ /10% He). A residual of a few percent of  $N_2$  is always present in the gas mixtures since the  $CH_4$  certified cylinders were buffered in nitrogen. Error bars shown on the plot correspond to the standard deviation of the PA signal recorded in a 5-min period. Lines are the result of a fit by a linear function for  $N_2$ , He and  $O_2$ /He mixture, and by the sum of a linear and a quadratic term for  $O_2$

relaxation effects. With the adjunction of only 10% of helium, the signal measured in  $O_2$  reaches almost the same level as in pure He. The  $O_2^*(\nu)$  relaxation rate in an  $O_2$ –He mixture may be calculated according to Eq. (3): with 10% of helium, it decreases from 15 ms (in  $O_2$ ) to 0.4 ms, which becomes smaller than the laser modulation period. Consequently, the absorbed laser energy fully contributes to the generation of the PA signal and the usual behaviour is again observed (linear variation of the PA signal with the  $CH_4$  concentration). This positive influence of helium makes possible the detection of methane at sub-ppm level for process control in the manufacturing of the ZWPFs.

## 5 Conclusion

The importance of collisional relaxation processes in the PA signal generation has been demonstrated in the particular case of  $CH_4$  detection in dry  $O_2$  and  $O_2$ – $N_2$  mixtures. A negative influence of molecular relaxation effects has been observed, which resulted in a strongly reduced and phase-shifted PA signal. The origin of this phenomenon lies in the existence of a fast resonant V–V coupling between  $CH_4^*(\nu_4)$  and  $O_2^*(\nu)$  vibrational states, associated with a small V–T relaxation rate of the  $O_2^*(\nu)$  excited state. This effect is independent of the frequency of the excited  $CH_4$  transition and is therefore expected to occur with any laser source used for the detection of  $CH_4$  in  $O_2$ / $N_2$  mixtures by PAS. This has been confirmed by our experimental results obtained in two different NIR absorption bands of methane ( $2\nu_3$  at 1.65  $\mu\text{m}$  and  $\nu_1 + \nu_4$  at 2.37  $\mu\text{m}$ ) using two types of semiconductor DFB lasers.

A qualitative theoretical explanation of the relaxation phenomena involved in our experimental observations has been proposed. However, the relaxation rates calculated from data reported in the literature for different processes connected with the considered system are much smaller than the values estimated from the experimental measurements. This discrepancy shows that the proposed model is only a qualitative description of the observed phenomena and is not able to predict quantitative data, such as an accurate value of the amplitude or phase of the generated PA signal. Other relaxation processes that were not taken into account probably also contribute to the PA signal. The proposed model is also only a qualitative model of the relaxation phenomena and cannot describe the full process of PA signal generation.

The beneficial effect of several species acting as a catalyst that promotes the V–T relaxation of the  $CH_4$ – $O_2$  system has been demonstrated. Among these substances, methane itself is one of the most efficient. As a result, an unusual parabolic variation of the PA signal with the  $CH_4$  concentration has been observed. A non-linear response with respect to the concentration of the target species has already been reported in PAS in the case of a gas mixture containing several species diluted in a  $N_2$ / $O_2$  carrier gas. A well-known case occurs for the detection of  $NH_3$  in a sample containing  $NH_3$ ,  $CO_2$  and  $H_2O$  in a  $N_2$ / $O_2$  buffer gas [27]. Although this situation is also induced by relaxation effects (kinetic cooling of  $CO_2$ ), the non-linear response was produced in that case by the superposition of several PA signals with a different phase. The behaviour reported here is different, as the observed parabolic response occurs for a single species ( $CH_4$ ) diluted in a  $N_2$ / $O_2$

buffer gas. This parabolic response results from a double-linear dependence of completely different origin. In addition to the usual linear response of the PA signal with respect to the gas concentration (due to the increasing amount of energy absorbed in the sample), a second linear variation is induced by relaxation effects. Other species that have shown a beneficial effect on the V–T relaxation of the CH<sub>4</sub>–O<sub>2</sub> system are water vapour and helium. An absolute humidity rate of 1% (corresponding to a relative humidity of 100% at 7 °C or 50% at 18 °C) or a helium concentration of around 10% in a O<sub>2</sub>/N<sub>2</sub> mixture has been shown to be sufficient to suppress the undesirable influence of molecular relaxation in our sensor, operated at atmospheric pressure and using a modulation frequency in the kHz range. However, a higher concentration of these species is required to obtain a similar result if a larger modulation frequency or a reduced pressure is considered.

The dramatic reduction of the methane PA signal generated in O<sub>2</sub> and its high dependence on the humidity rate were also observed in O<sub>2</sub>/N<sub>2</sub> mixtures containing only a few percent of O<sub>2</sub>. Therefore, this phenomenon may also affect the monitoring of methane in ambient air (21% of O<sub>2</sub>) by PAS, for example for atmospheric researches or greenhouse gases emission monitoring. This effect must be considered especially when working in relatively dry conditions, which certainly occurs for field measurements during winter time, or when measurements are performed at reduced pressure (at altitude, for example). The positive effect of He also makes our PAS-based sensor suitable for sub-ppm CH<sub>4</sub> detection for process control in the manufacturing of the novel LWPFs. Without this beneficial influence, the monitoring of methane by PAS in this application would not be possible, due to the strongly reduced sensitivity induced by relaxation effects.

**ACKNOWLEDGEMENTS** The authors would like to acknowledge the Commission of Technology and Innovation of the Swiss Government for financial support (through Contract No. 6273.1-KTI) and the companies Omnisens SA and Daetwyler Fiber Optics SA for their technical and financial contributions. The authors are also grateful to C. Boursier (Université Pierre et Marie Curie, Paris) for fruitful discussions about methane relaxation in oxygen.

## REFERENCES

- P.L. Meyer, M.W. Sigrist, *Rev. Sci. Instrum.* **61**, 1779 (1990)
- M.W. Sigrist, *Infrared Phys. Technol.* **36**, 415 (1995)
- S. Schilt, L. Thévenaz, M. Niklès, L. Emmenegger, C. Hügli, *Spectrochim. Acta A* **60**, 3259 (2004)
- M.B. Pushkarsky, M.E. Webber, O. Baghdassarian, L.R. Narasimhan, C.K.N. Patel, *Appl. Phys. B* **75**, 391 (2002)
- Z. Bozóki, Á. Mohácsi, G. Szabó, Zs. Bor, M. Erdélyi, W. Chen, F.K. Tittel, *Appl. Spectrosc.* **56**, 715 (2002)
- A.D. Wood, M. Camac, E.T. Gerry, *Appl. Opt.* **10**, 1877 (1971)
- M. Hammerich, A. Ólafsson, J. Henningsen, *Chem. Phys.* **163**, 173 (1992)
- A. Veres, Z. Bozóki, Á. Mohácsi, M. Szakáll, G. Szabó, *Appl. Spectrosc.* **57**, 900 (2003)
- A.A. Kosterev, Y.A. Bakhirkin, R.F. Curl, F.K. Tittel, *Opt. Lett.* **27**, 1902 (2002)
- A.A. Kosterev, Y.A. Bakhirkin, F.K. Tittel, *Appl. Phys. B* **80**, 133 (2005)
- A.A. Kosterev, F.K. Tittel, *Appl. Opt.* **43**, 6213 (2004)
- K. Kincade, *Laser Focus World* **39**(3), 97 (2003)
- C.F. Dewey, in: *Optoacoustic Spectroscopy and Detection*, ed. by Y.-H. Pao (Academic, New York 1977), Chap. 3, pp. 47–77
- C. Boursier, J. Ménard, L. Doyennette, F. Menard-Bourcin, *J. Phys. Chem. A* **107**, 5280 (2003)
- L. Doyennette, F. Menard-Bourcin, J. Ménard, C. Boursier, C. Camy-Peyret, *J. Phys. Chem. A* **102**, 3849 (1998)
- H.E. Bass, H.-J. Bauer, *Appl. Opt.* **12**, 1506 (1973)
- J.T. Yardley, C.B. Moore, *J. Chem. Phys.* **48**, 14 (1968)
- D.L. White, *J. Chem. Phys.* **42**, 2028 (1965)
- D.L. White, R.C. Millikan, *J. Chem. Phys.* **39**, 1807 (1963)
- J.-P. Besson, S. Schilt, L. Thévenaz, *Spectrochim. Acta A* **60**, 3449 (2004)
- S. Schilt, J.-P. Besson, L. Thévenaz, Fiber-coupled photoacoustic sensor for sub-ppm methane monitoring, in: *Proceedings of the Second European Workshop on Optical Fiber Sensors* (SPIE Proc. volume 5502), ed. by J.M. López-Higuera, B. Culshaw (SPIE, Bellingham, WA 2004), pp. 317–320
- S. Schilt, L. Thévenaz, *Infrared Phys. Technol.*, in press, DOI: 10.1016/j.infrared.2005.09.001
- V. Zéninari, B. Parvitte, D. Courtois, V.A. Kapitanov, Y.N. Ponomarev, *Appl. Phys. B* **72**, 953 (2001)
- F. Menard-Boucin, C. Boursier, L. Doyennette, J. Menard, *J. Phys. Chem. A* **105**, 11446 (2001)
- S. Schilt, A. Vicet, R. Werner, M. Mattiello, L. Thévenaz, A. Sahli, Y. Rouillard, J. Koeth, *Spectrochim. Acta A* **60**, 3431 (2004)
- F.G.C. Bijnen, F.J.M. Harren, J.H.P. Hackstein, J. Reuss, *Appl. Opt.* **35**, 5357 (1996)